J. Phys. B: At. Mol. Opt. Phys. 27 (1994) 3891–3904. Printed in the UK

Autoionization of low-lying 5d*n*g states in barium

Robert van Leeuwen, Wim Ubachs and Wim Hogervorst

Laser Centre Vrije Universiteit Amsterdam, Department of Physics and Astronomy, De Boelelaan 1081, 1081 HV Amsterdam, The Netherlands

Received 4 May 1994

Abstract. The autoionizing 5d*n*g $J=1$–5 states in barium for $n=5$–8 were investigated in a two-step pulsed laser atomic beam experiment. The wavefunctions of the 5d*n*g configuration can be well described in a $(jl)K$-coupled basis. Each 5d,*n*g[K] fine structure state autoionizes into a single 6sεl continuum channel. Autoionization rates, deduced from observed linewidths, are found to be symmetrically lower than values calculated using a single configuration approximation. The fine structure dependence of the autoionization rates, however, can be reproduced in these calculations.

1. Introduction

In recent years rapid progress has been made in the understanding and quantitative modelling of autoionization processes in two-electron systems. Experimentally multi-step laser excitation of the heavier earth-alkaline atoms resulted in a wealth of data on doubly-excited configurations, particularly for the barium atom (Dai *et al* 1989, Pruvost *et al* 1990, De Graaff *et al* 1992, Wang and Cooke 1993). Multi-channel quantum defect theory (MQDT) in combination with eigenchannel R-matrix calculations (Greene and Kim 1987, Aymar 1990, Greene and Aymar 1991) is quite successful in describing autoionizing spectra of these atoms even in cases involving large numbers of continuum channels (Luc-Koenig *et al* 1994, Lecomte *et al* 1994). In such a semi *ab initio* approach model potentials are used that are adjusted to the ionic spectrum for each value of the orbital angular momentum l.

Nikitin and Ostrovsky (1980) developed an analytical framework to calculate autoionization rates in two-electron systems using single configuration wavefunctions. Its applicability is limited to doubly-excited states where the outer electron has a large orbital angular momentum ($l \geqslant 3$). Poirier (1988) included core polarization effects in the model of Nikitin and Ostrovsky and introduced numerical calculation of radial matrix elements. Recently the model was tested in the 6p*n*f manifold of barium for $J=1$–5 total angular momentum Rydberg series (Abutaleb *et al* 1991). Experimentally the autoionization rates of the 6p*n*f J states were found to be up to a factor of two larger than calculated values. Accounting for $6p_{3/2}nf$–$6p_{1/2}\varepsilon l$ fine structure autoionization resulted in only minor changes of the order of 10–20% in the rates of autoionization. Poirier (1988) compared his calculation of autoionization rates of $6p_{3/2}ng$ $J=5$ levels with experimental linewidths measured by Jaffe *et al* (1985). For the $K=\frac{9}{2}$ level good agreement was found but for the $K=\frac{11}{2}$ level the calculated autoionization rate was found to be three times lower than the experimental value.

0953-4075/94/173891+14$19.50

In the present work the Nikitin–Ostrovsky and Poirier model for autoionization is applied to an example that is simple in many respects. The outer electron in the 5d*n*g states of barium is in a non-penetrating orbit. Also there is no overlap with the inner 5d valence electron. Therefore exchange effects in the autoionization process may be ignored and the autoionization rate is determined solely by the long range (direct) electrostatic interaction. 5d*n*g states below the $5d_{3/2}$ ionization limit, which only decay into 6sεl continua, were studied. As autoionization rates of the 5d*n*g series are low the present investigation was limited to low-n configurations in order to avoid laser linewidth effects on the observed transitions. Only the $n=5$–8 configurations were excited as well as several components of $n=10$ ($K=\frac{7}{2}, \frac{9}{2}$). The 5d*n*g configuration is found to be purely $(jl)K$-coupled. No contribution to the fine structure due to the spin of the outer 5g electron is found to occur. Each 5d*n*g [K] state can only couple to a single 6sεl continuum, thereby drastically simplifying the problem. In the present work observed autoionization rates, as determined from linewidth measurements, are compared with calculations. Notwithstanding the fact that the model should be applicable straightforwardly for the 5d*n*g configuration experimental rates of autoionization are a factor of five lower than calculated values.

The present investigation of 5d*n*g states in barium is stimulated by the possibility to use these states as intermediates for the excitation of higher lying doubly-excited states where both electrons have a large orbital angular momentum (Jones *et al* 1991). Here we analyse seven out of ten possible components of the 5d*n*g [K] multiplet. A comparison is made with results of Bente and Hogervorst (1989a) for 5d*n*g series for high values of n.

2. Experimental method

The low lying autoionizing 5d*n*g states of barium were excited in a two-step pulsed laser experimental. The excitation scheme, with relevant energy levels, is given in figure 1. A first dye laser in the wavelength region 650 nm–730 nm using DCM or LDS dyes, was pumped by the second harmonic output (532 nm) of a Nd:YAG laser with a repetition rate of 10 Hz. Its frequency ν_1, with bandwidth $\Delta\nu_1=0.3\ \text{cm}^{-1}$, was tuned to the selected 6s5d–5d6p transitions. The second dye laser was pumped by either the second or the third harmonic output (355 nm) of the same Nd:YAG laser depending on the dye required to excite the 5d*n*g states. The dye laser frequency ν_2, with bandwidth $\Delta\nu_2=0.07\ \text{cm}^{-1}$, was scanned in steps of about $0.02\ \text{cm}^{-1}$ over the 5d6p–5d*n*g transitions. The two counterpropagating laser beams were spatially overlapped in the interaction region perpendicularly intersecting an atomic beam between two closely spaced (1 cm) capacitor plates at zero potential. After a time delay of 0.5 μs a voltage pulse of -200 V was applied to one of the plates. The produced ions were collected and directed through a grid towards an electron multiplier. The ion signal was processed via a boxcar integrator and stored on a computer. At each wavelength setting the signal of 10 laser shots was summed. The atomic beam was produced by heating a sample of natural barium in a small tantalum oven using a tungsten heating wire. To populate the metastable 6s5d $^1D_2$, $D_{1,2,3}$ levels a low voltage discharge (<10 V, 800 mA) was maintained between oven and heating wire. The population of 6s5d metastable states is estimated to be 1%.

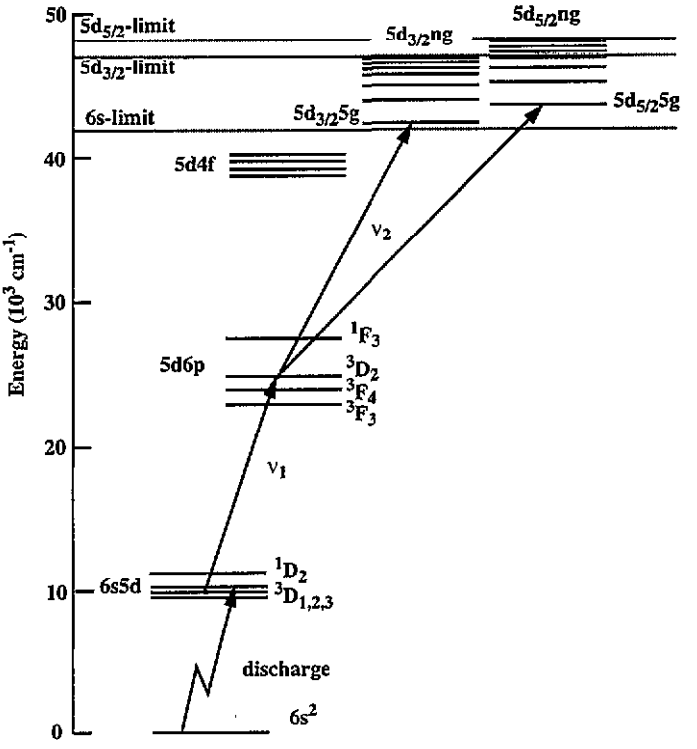

Figure 1. Energy level diagram showing the two-step excitation scheme of 5d*n*g states.

The goal of the experiment was to determine autoionization rates of the 5d*n*g states from linewidth measurements, so great care was taken to avoid additional line broadening effects. The pulse of the second dye laser arrived about 7 ns after the first laser pulse, while pulse durations were about 4–5 ns. Thus coherent two-photon excitation was avoided and the linewidth was determined by the (narrow) bandwidth of the second dye laser only. The laser power of the first dye laser was reduced to about 50 μJ per pulse such that multiphoton ionization with the first dye laser alone did not occur. Furthermore the laser power of the second dye laser was reduced until power broadening effects were clearly absent. Energy positions of the 5d*n*g resonances were determined using a home-built echelle-grating wavelength meter yielding an accuracy of about 0.10 cm^{-1}. With an additional uncertainty of 0.05 cm^{-1} in the level energies of the intermediate 5d6p configuration (Vergès 1984), a small uncertainty resulting from the procedure used to fit the (Voigt or Fano) line shapes and non-linearities in the laser scan the total uncertainty in the 5d*n*g level energies is estimated to be 0.15 cm^{-1}.

3. Theoretical framework

The calculation of autoionization rates and fine structure of the 5d*n*g configuration is based on a simple model of an atom with two valence electrons in a doubly-excited state. This model assumes that the outer valence electron (1) on the average is much further away from the 2^+ core than the inner valence electron (2). The Hamiltonian

can then be written in the form:

$$H = H_0 + H_{so} + V \tag{1a}$$

with

$$H_0 = \frac{p_1^2 + p_2^2}{2} - \frac{2}{r_2} - \frac{1}{r_1} \tag{1b}$$

and

$$V = \frac{1}{r_{12}} - \frac{1}{r_1} \tag{1c}$$

where r_i and p_i are the radial position and momentum of electron i. H_{so} represents the spin–orbit interaction of both valence electrons. The Coulomb repulsion, $1/r_{12}$, between the two valence electrons is responsible for autoionization as well as for fine structure splitting.

An atom in a doubly-excited $n_2 l_2 n_1 l_1$ state interacting with $n_0 l_0 \varepsilon l$ continuum states of the same parity and the same value of the total angular momentum J will autoionize. This results in an ion in a $n_0 l_0$ state and an ejected electron with energy ε, determined by energy conservation, and angular momentum l. The autoionization rate Γ is given by:

$$\Gamma = 2\pi |\langle n_0 l_0 \varepsilon l J | V | n_2 l_2 n_1 l_1 J \rangle|^2. \tag{2}$$

Similarly the fine structure splitting within a configuration due to the electrostatic repulsion is given by a matrix element involving the same operator:

$$W_{ES}^{split} = \langle n_2 l_2 n_1 l_1 J | V | n_2 l_2 n_1 l_1 J \rangle. \tag{3}$$

To evaluate these matrix elements the Coulomb repulsion term in the perturbation V can be expanded in multipoles:

$$\frac{1}{r_{12}} = \sum_{k=0}^{\infty} \frac{r_<^k}{r_>^{k+1}} C_1^{(k)} C_2^{(k)} \tag{4}$$

where $C_1^{(k)}$ and $C_2^{(k)}$ are spherical harmonic vector operators and $r_>(r_<)$ is the larger (smaller) of the radial positions (r_1, r_2). In the 5dng as well as in the continuum configurations the inner electron at r_2 may be assumed to always be closer to the core than the outer electron at r_1, thus simplifying the evaluation of equation (4). The zero-order term in equation (4) is cancelled by the $1/r_1$ term in equation (1c).

If configuration interaction is ignored single configuration wavefunctions can be used. Antisymmetrization of the wavefunctions results in a direct and an exchange contribution to the matrix elements. The exchange parts can be neglected when the outer electron is in a high-l state ($l \geqslant 3$), because of the small overlap of its wavefunction with the inner valence electron. Since the wavefunctions are, for high-l states, best described in a $(jl)K$-coupling scheme and the electrostatic interaction between the valence electrons is diagonal with respect to K, it is convenient to calculate the matrix elements for the direct autoionization rate and the fine structure splittings for $(jl)K$-coupled states.

3.1. Fine structure

The first order contribution to the fine structure splitting of a $(jl)K$-coupled configuration is caused by the spin–orbit interaction of the inner electron. For the 5dng configuration the $5d_{3/2}ng$ and $5d_{5/2}ng$ levels are separated by 801.0 cm^{-1}. The second order contribution, W_{ES}^{split}, further splits the $5d_jng$ levels into K-components and may be written as (Cowan 1981):

$$W_{ES}^{split}=\sum_k f_k F^{(k)} \qquad k=2,4 \tag{5}$$

where f_k represents angular coefficients and $F^{(k)}$ are the so called direct radial Slater integrals which can, using the assumptions made above, be written:

$$F^{(k)}=\langle 5d|r^k|5d\rangle\langle ng|1/r^{k+1}|ng\rangle. \tag{6}$$

The one-electron radial integrals may be evaluated using well known analytical expressions for the expectation values of r^k (Cowan 1981). The 5d electron is assumed to move in the field of a $Z=2$ core. Core penetration is accounted for by replacing the principal quantum number n by an effective quantum number $n^*=n-\delta$, where δ is the quantum defect of the 5d electron in the Ba^+ ion ($\delta=2.59$). For the ng electron hydrogen wavefunctions are taken. The calculated Slater integrals $F^{(2)}$ and $F^{(4)}$ are given in table 1. The angular coefficients f_2 and f_4 are evaluated in a $(jl)K$ coupling scheme. The fine structure of the 5dng configuration then follows through equation (5).

Table 1. Slater–Condon parameters as obtained from a least squares analysis including 7 out of 10 $5d_jng$ K levels for $n=5$–8. Calculated values for the second and fourth order direct radial integrals are included as well. All values in cm^{-1}.

		F^2		F^4	
	E_{av}	exp.	calc.	exp.	calc.
5d5g	42 969.9 (4)	155 (3)	170.3	10 (9)	10.7
5d6g	44 321.0 (5)	81 (3)	98.7	20 (8)	7.9
5d7g	45 136.7 (3)	50 (3)	62.1	10 (9)	5.6
5d8g	45 665.0 (2)	28 (2)	41.6	—	3.9

3.2. Autoionization

With the assumptions made earlier the autoionization rate for an atom in a $(jl)K$-coupled doubly-excited $n_2l_2n_1l_1$ state ionizing into a $n_0l_0\varepsilon l$ continuum can be expressed as follows:

$$\Gamma_K=2\pi[l_2,l_1,l_0,l,j_0,j_2]\sum_{k\geqslant 1}\begin{pmatrix}l_0 & k & l_2\\ 0 & 0 & 0\end{pmatrix}^2\begin{pmatrix}l & k & l_1\\ 0 & 0 & 0\end{pmatrix}^2\begin{Bmatrix}l_0 & s & j_0\\ j_2 & k & l_2\end{Bmatrix}^2\begin{Bmatrix}j_0 & l & K\\ l_1 & j_2 & k\end{Bmatrix}^2$$

$$\times\langle n_0l_0|r^k|n_2l_2\rangle^2\langle\varepsilon l|r^{-k-1}|n_1l_1\rangle^2 \tag{7}$$

$[l_2, l_1, \ldots]$ stands for $(2l_2+1)$ $(2l_1+1)$ etc. The autoionization rate is independent of the value of J. To calculate the matrix element $\langle\varepsilon l|r^{-k-1}|n_1l_1\rangle$ the outer Rydberg

electron is represented by a hydrogen wavefunction. For the continuum wavefunction of the ejected electron a regular Coulomb wavefunction is used:

$$R_{\varepsilon l}(r) = c_{pl}(2pr)^l \, \mathrm{e}^{-\mathrm{i}pr} \, {}_1F_1(l+1+\mathrm{i}/p;\, 2l+2;\, 2\mathrm{i}pr) \tag{8a}$$

where

$$c_{pl} = \sqrt{\frac{2p}{\pi}} \frac{|\Gamma(l+1-\mathrm{i}/p)|}{\Gamma(2l+2)} \, \mathrm{e}^{\pi/2p}. \tag{8b}$$

${}_1F_1$ is the confluent hypergeometric function, Γ the Gamma function and p the momentum of the ejected electron, $p=(2\varepsilon)^{1/2}$. For circular states ($n_1 = l_1 + 1$) an analytic expression for the radial matrix element can be derived (Nikitin and Ostrovsky 1980):

$$\langle \varepsilon l | r^{-k-1} | n_1 l_1 \rangle = \frac{c_{pl}(2p_1)^{l_1+3/2}}{\sqrt{\Gamma(2l_1+3)}} (2p)^l \Gamma(l+l_1-k+2)(p_1+\mathrm{i}p)^{-l-l_1+k-2}$$

$$\times \, {}_2F_1(l+1+\mathrm{i}/p,\, l+l_1-k+2;\, 2l+2;\, 2\mathrm{i}p/(p_1+\mathrm{i}p)) \tag{9}$$

where ${}_2F_1$ stands for the hypergeometrical function and $p = 1/n_1$ is the momentum of the $n_1 l_1$ electron.

The $5d_j ng$ states of barium investigated in this work all lie below the $5d_{3/2}$ ionization limit and therefore only autoionize into $6s_{1/2}\varepsilon l$ continua. Autoionization entirely occurs via quadrupolar coupling between $5dng$ and $6s\varepsilon l$ states since only the second order term ($k=2$) in equation (7) is non-zero. The values of the angular momentum of the ejected electron are restricted to $l=2$, 4 or 6. From angular momentum selection rules it follows that the $5d_j5g$ $K=\frac{3}{2}$ and $\frac{5}{2}$ levels couple to $6s_{1/2}\varepsilon d$ continua, $5d_j5g$ $K=\frac{7}{2}$ and $\frac{9}{2}$ to $6s_{1/2}\varepsilon g$ continua and $K=\frac{11}{2}$ and $\frac{13}{2}$ couple to $6s_{1/2}\varepsilon i$ continua while K is conserved. So each initial $5dng$ state can autoionize only into a single continuum. This greatly simplifies the calculation of autoionization rates. For the specific case of autoionization of $5d_j ng$ states into $6s_{1/2}\varepsilon l$ continua equation (7) reduces to:

$$\Gamma_K^{5d_j ng \to 6s_{1/2}\varepsilon l} = \tfrac{18}{5}\pi(2l+1)(2j_2+1) \begin{pmatrix} l & 2 & 4 \\ 0 & 0 & 0 \end{pmatrix}^2 \begin{Bmatrix} \frac{1}{2} & l & K \\ 4 & j_2 & 2 \end{Bmatrix}^2 \langle 6s|r^2|5d\rangle^2 \langle \varepsilon l|r^{-3}|ng\rangle^2 \tag{10}$$

where $K = l \pm \frac{1}{2}$ and $l=2$, 4, 6. Since the $5d_j ng$ states are $(jl)K$ coupled equation (10) can be directly applied to calculate the autoionization rates of the various K levels. The quadrupole matrix element is taken from Poirier (1993), who recently calculated $\langle 6s|r^2|5d\rangle$ to be 14.01 a_0^2 by numerical integration of the one-electron Schrödinger equation. He followed a Numerov procedure and accounted for core-polarization effects.

For the 5d5g configuration the radial matrix element $\langle \varepsilon l|r^{-3}|5g\rangle$ can be calculated from equation (9) since the outer electron is in a circular state ($n_1 = l_1 + 1$). The $5d_{3/2}5g$ levels produce electrons with less energy ($p=0.066$ au) than the $5d_{5/2}5g$ levels ($p=0.107$ au). As the production of slow electrons is favoured the autoionization width of

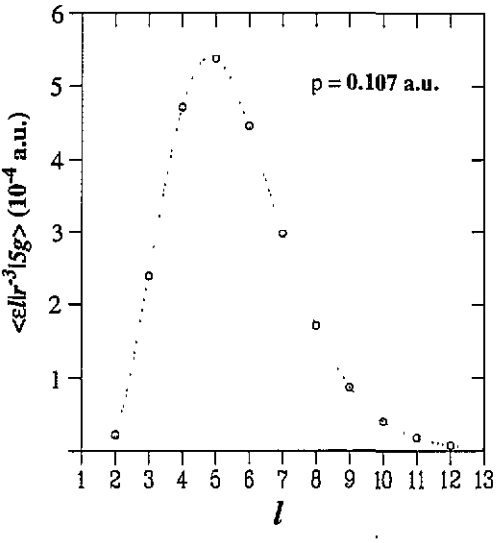

Figure 2. Dependence of the radial matrix element $\langle \varepsilon l | r^{-3} | 5g \rangle$ on the orbital angular momentum l of the ejected electron as calculated from equation (8). The momentum p of the ejected electron is determined from energy conservation, $\varepsilon = p^2/2$.

the $5d_{3/2}ng$ levels is larger by about 5%. In figure 2 the radial matrix element involving a $5d_{5/2}5g$ state is given as a function of the angular momentum l.

The radial matrix element $\langle \varepsilon l | r^{-3} | ng \rangle$ for $n > 5$ cannot be obtained by simple n^{-3} scaling of the matrix element. The autoionization rate Γ strongly depends on the overlap of the electron wavefunctions at small r. For $n \gg l$ the classical inner turning point of the outer electron r_i is independent of n, $r_i \approx \frac{1}{2} l(l+1)$ and Γ is therefore proportional to the number of roundtrips per unit time of the electron ($n^3\Gamma = \text{constant}$). For low n, however, r_i increases with decreasing n, which results in a lower value of the scaled autoionization rate $n^3\Gamma$. Instead the radial integrals have to be calculated by numerical integration. In figure 3 calculated scaled autoionization widths of $5d_{5/2}ng$ $K = \frac{9}{2}$ levels are plotted versus n. It shows that the n^{-3} scaling of the autoionization rate is not valid for low n (<10). The calculated value of the scaled autoionization rate for large n is in agreement with the value, transferred from LS- to jl-coupling, calculated by Poirier (1988) for 5d24g $L = 4$.

4. Results and interpretation

4.1. Observed spectra

Low-lying 5dng configurations ($n = 5$–8) of barium above the first (6s) ionization limit at 42 034.90 cm^{-1}, but still below the $5d_{3/2}$ ionization limit at 46 908.75 cm^{-1}, were studied. The 5dng $J = 1$–5 states, excited via 5d6p $^3D_2$, $^{1,3}F_3$, $^3F_4$ intermediate states (see figure 1) appeared as closely spaced narrow resonances, have a small quantum defect and lie between broad 5dns and 5dnd resonances. Figure 4(a) shows an example of a recorded $5d_{5/2}5g$ spectrum excited from the 5d6p $^3F_4$ level at 23 757.03 (5) cm^{-1}. Only three resonances were observed, identified in a (jl)K-coupling scheme as $K = \frac{9}{2}$, $K = \frac{7}{2}$ and $K = \frac{5}{2}$ levels. The $K = \frac{11}{2}$ $J = 5$ level was not observed. In the spectrum of figure 4(b)

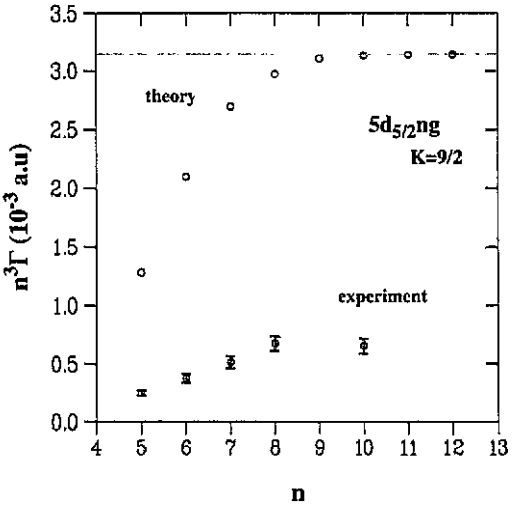

Figure 3. Scaled autoionization rates for the $5d_{5/2}ng$ $K=\frac{9}{2}$ states as a function of n. The calculated values are obtained by numerically integrating the radial integral of the outer electron.

$5d_{5/2}5g$ states, excited from the $5d6p\ ^3D_2$ level at 24 531.49 (5) cm^{-1}, are shown. Splittings of K-components in two J-components ($J=K\pm\frac{1}{2}$) were not observed. Many spectra of various fine structure components of the $5dng$ ($n=5$–8) configurations were recorded. The observed $5dng$ resonances vary in lineshape, linestrength and linewidth.

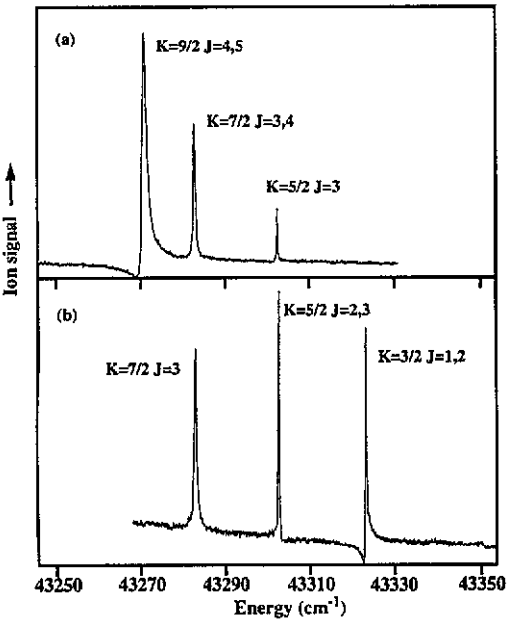

Figure 4. Specta of the low-lying $5d_{5/2}5g$ state in barium excited (*a*) via $5d6p\ ^3F_4$ and (*b*) via $5d6p\ ^3D_2$. The 5d5g resonances are identified in a $(jl)K$-coupling scheme.

Symmetric Voigt profiles as well as asymmetric Fano profiles are observed. The appearance of Fano profiles may results from interaction of 5d*n*g states with broad 5d*nl* ($l=0, 2$) autoionizing resonances or with 6sεl continua with equal value of the total angular momentum J. The 5d*n*s and 5d*n*d resonances can be excited directly from the 5d6p configuration, while excitation of 6sεl results from an admixture of odd-parity 6s*nl* character in 5d6p.

4.2. Fine structure analysis

The analysis of the multiplet structure of the 5d*n*g configurations is based on a Slater–Condon type of analysis incorporating the accurately measured level energies of 5d*n*g resonances. Observed line intensities are used to find the correct J-assignment of the K-levels in the spectra. As 5d*n*g states cannot be excited from a pure 5d6p configuration for a fine structure analysis two assumptions have to be made that will be proven valid *a posteriori*. First configuration interaction of 5d6p and 5d4f is assumed to be responsible for the excitation of 5d*n*g resonances. Secondly the 5d*n*g configuration is considered to be $(jl)K$ coupled.

Line intensities in the 5d6p–5d*n*g multiplet were calculated based on the assumption of 5d6p–5d4f configuration mixing. The intermediate 5d6p configuration is described well in a LS-coupling scheme (Grundevik *et al* 1982). Since the Coulomb interaction is diagonal in LS-coupling and because the energy separation between the 5d6p and 5d4f configurations is much larger (about 15 000 cm^{-1}) than the internal splittings in the (jj-coupled) 5d4f configuration, the 5d4f fraction in the 5d6p wavefunction can also be treated as LS-coupled. Relative transition probabilities from LS-coupled 5d4f levels to jl-coupled 5d*n*g levels were calculated and are listed in table 2.

Table 2. Calculated relative linestrengths for the 5d6p–5d*n*g transition. These transitions are assumed to be possible due to configuration mixing of 5d4f and 5d6p states. The 5d4f fraction in the 5d6p wavefunctions was assumed to be LS-coupled while the 5d*n*g levels are $(jl)K$-coupled.

final $5d_j ng$ state			initial 5d6p state			
j_{5d}	K	J	$^3F_4$	$^3F_3$	$^1F_3$	$^3D_2$
3/2	11/2	5	0.0000			
3/2	9/2	5	0.2801			
3/2	9/2	4	0.0064	0.0955	0.1273	
3/2	7/2	4	0.0331	0.3175	0.2001	
3/2	7/2	3	0.0009	0.0000	0.0446	0.1020
3/2	5/2	3	0.0010	0.0365	0.0248	0.1837
3/2	5/2	2		0.0006	0.0032	0.0000
5/2	11/2	5	0.0000			
5/2	9/2	5	0.7202			
5/2	9/2	4	0.0164	0.2455	0.3274	
5/2	7/2	4	0.2046	0.1228	0.1637	
5/2	7/2	3	0.0058	0.1137	0.0546	0.1247
5/2	5/2	3	0.0172	0.0478	0.0496	0.1372
5/2	5/2	2		0.0160	0.0016	0.0992
5/2	3/2	2		0.0042	0.0032	0.0496
5/2	3/2	1				0.0179

Table 3. Results of the fine structure analysis of the 5d5g multiplet. Average energy positions (with an uncertainty of 0.1 cm^{-1}) of the 5d$_j$5g K levels are determined from transitions from several intermediate 5d$_j$6p states. Exchange and spin–orbit interaction of the outer electron are neglected. The spin–orbit parameter of the inner electron is taken from the ion, $\xi_{5d} = 390.39\ cm^{-1}$. All values in cm^{-1}.

j_{5d}	K	J	Exp. energy	Fit	Δ (Exp. − Fit)
3/2	5/2	2, 3	42 509.92	42 511.17	−1.25
3/2	7/2	3, 4	42 480.06	42 480.29	−0.23
3/2	9/2	4, 5	42 470.83	42 469.54	+1.29
3/2	11/2	5, 6		42 500.35	
5/2	3/2	1, 2	43 323.43	43 322.52	+0.91
5/2	5/2	2, 3	43 302.95	43 302.56	+0.39
5/2	7/2	3, 4	43 283.10	43 283.47	−0.37
5/2	9/2	4, 5	43 271.02	43 271.76	−0.74
5/2	11/2	5, 6		43 274.81	
5/2	13/2	6, 7		43 306.42	

The observed 5dng resonances were assigned on the basis of predicted fine structure splittings and calculated line intensities. Experimental level energies of the 5d5g configuration are collected in table 3. The energies of 5d$_j n$g $[K]$ levels determined from transitions from various intermediate 5d6p states were averaged. The energies of 5d$_j n$g $J = K - \frac{1}{2}$ and $J = K + \frac{1}{2}$ levels were also averaged as no effect of the spin of the outer electron was observed. In none of the recorded spectra could splittings of K-components in separate J-components be observed. The transition probability to the $J = K - \frac{1}{2}$ level is usually much smaller than to the $J = K + \frac{1}{2}$ level as can be deduced from table 2, e.g. the transition probability to the $J = 4$ component of the $K = \frac{9}{2}$ state in figure 4(a) is about 2 orders of magnitude smaller than that to the $J = 5$ component, but it is still of the same order as the transition probability to the $K = \frac{5}{2}$ $J = 3$ level which could be observed. The $K = \frac{9}{2}$ peak in figure 4(a) can be assigned to have $J = 5$. The $K = \frac{9}{2}$, $J = 4$ levels were excited separately from a 5d6p $J = 3$ state. The energy positions of both $K = \frac{9}{2}$ levels, excited through different excitation schemes, coincide within the experimental error.

Experimental values for the Slater parameters were determined in a least-squares minimization routine, including 7 out of the possible 10 5d$_j n$g K-levels. The average energy of the multiplet and the values of the Slater parameters $F^{(2)}$ and $F^{(4)}$ of the 5dng $n = 5$–8 configurations resulting from this procedure are collected in table 1. The spin–orbit parameter of the inner electron was taken from the Ba^+ ion, $\xi_{5d} = 320.39\ cm^{-1}$. The $F^{(2)}$ parameters obtained from the fit scale as n_g^{-3} and differ not more than 30% with the calculated values. Calculated level energies of the 5d5g configuration and differences with observed values are included in table 3. Exclusion of the 5d$_{3/2}$5g $K = \frac{5}{2}$ and $K = \frac{9}{2}$ levels had a drastic effect on the value of the χ^2, reducing it from 10 to 0.2. The $K = \frac{5}{2}$ and $K = \frac{9}{2}$ levels appear to be slightly perturbed and shifted by about $2\ cm^{-1}$.

From this Slater–Condon multiplet analysis also the composition of the wavefunctions is obtained, and they are found to be over 99.6% pure on a $(jl)K$ basis. If the oscillator strengths are integrated over the line profiles the observed relative line intensities are in reasonable agreement with the calculated values from table 2. This confirms the assumption that 5d6p–5dng transitions are allowed due to configuration mixing of

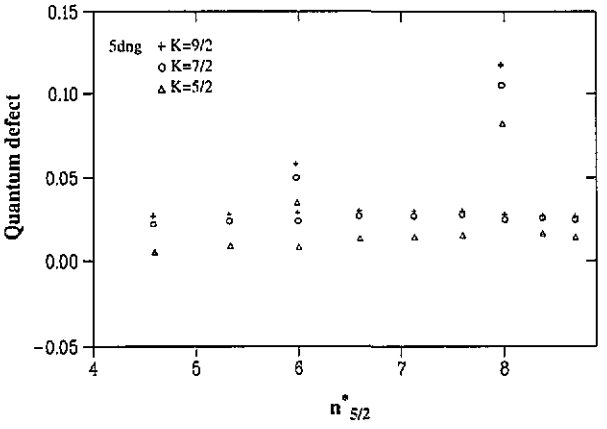

Figure 5. Quantum defect plot of 5dng $K=\frac{5}{2}, \frac{7}{2}$ and $\frac{9}{2}$ states below the $5d_{3/2}$ ionization limit. The quantum defects are calculated with respect to the $5d_{3/2}$ limit. The effective principal quantum number relative to the $5d_{5/2}$ limit, $n^*_{5/2}$, is used as a scaled energy axis. The 5dng states with $n \geqslant 9$ were observed by Bente and Hogervorst (1989). The $5d_{3/2}ng$ states appear as series with a small, almost constant quantum defect. The $5d_{5/2}ng$ states, although close to $5d_{3/2}n'g$ states for $n=6$ and $n=8$, do not perturb the $5d_{3/2}ng$ series.

5d6p and 5d4f states. The present results are consistent with observations of Camus *et al* (1983) for 5dng $J=1, 2$ ($n=5$–27) and of Bente and Hogervorst (1989a) for 5dng $J=2$–4 ($n \geqslant 9$). In figure 5 quantum defects of observed 5dng states, calculated with respect to the $5d_{3/2}$ limit, are plotted against the effective principal quantum number relative to the $5d_{5/2}$ limit. The 5dng states with $n \geqslant 9$ are taken from Bente and Hogervorst, the quantum defects are small (<0.03) and almost independent of energy. Interaction between $5d_{3/2}ng$ and $5d_{5/2}ng$ series is absent.

4.3. Experimental autoionization rates

The observed 5dng resonances display either a Lorentzian or a Fano line profile. Autoionization rates were determined from observed linewidths by deconvoluting a Gaussian laser profile (bandwidth 0.07 cm^{-1}). Only those recordings were considered where only a single J component of the 5d$_j ng$ [K] level contributes to the line intensity. In cases where two J levels could be excited even the smallest splitting of the K levels (for which no conclusive evidence was found) may contribute to the observed linewidths. In the example of $5d_{5/2}ng$ $K=\frac{5}{2}$ both $J=2$ and $J=3$ substates can be excited with almost equal strength from the 5d6p $^3D_2$ level (see table 2). When the narrow $K=\frac{5}{2}$ resonance (0.10 cm^{-1}) in figure 4(b) is fitted with a doublet of a Lorentz and a Fano profile, both of laser linewidth, instead of with a single Fano profile, a significant improvement results. The Fano profile may arise from interaction with a broad 5dnl ($l=0, 2$) $J=2$ resonance which is also excited. Since the observed linewidths of the $K=\frac{3}{2}$ and $K=\frac{5}{2}$ levels are close to laser linewidth, only an upper limit for the autoionization rates can be given.

The linewidths of the 5d$_j$5g [K] levels are found to be independent of the value of J. For example the observed linewidth of the $5d_{5/2}5g$ $K=\frac{9}{2}$ $J=5$ level excited from the 5d6p $^3F_4$ state (0.44 cm^{-1}) equals, within error bars, the linewidth of the $5d_{5/2}5g$ $K=\frac{9}{2}$ $J=4$ level excited from the 5d6p $^3F_3$ state (0.42 cm^{-1}) and from the 5d6p $^1F_3$ state

Table 4. Observed and calculated autoionization rates for 5d$_j$5g [K] states in cm^{-1}. In the last column the ratio of theoretical and experimental values is given.

5d5g state		Decay			
j_{5d}	K	channel	Theory	Experiment	Ratio
5/2	3/2	6sεd	0.012	<0.04	
3/2	5/2	6sεd	0.0074	<0.02	
5/2	5/2	6sεd	0.0041	<0.03	
3/2	7/2	6sεg	1.96	0.34 (3)	5.8
5/2	7/2	6sεg	1.43	0.29 (3)	4.9
3/2	9/2	6sεg	1.00	0.18 (2)	5.6
5/2	9/2	6sεg	2.29	0.43 (4)	5.3
3/2	11/2	6sεi	2.90		
5/2	11/2	6sεi	0.45		
5/2	13/2	6sεi	2.42		

(0.44 cm^{-1}). For the other levels this agreement is also found. Therefore the autoionization rates of 5d$_j$5g K states are averaged over the J states. Values for each $(jl)K$-coupled level are given in table 4. The error is estimated to be 10% of the observed linewidth.

The strong dependence of the radial matrix element on l (see figure 2) explains the difference between the observed linewidth of the narrow $K=\frac{3}{2}$ and $K=\frac{5}{2}$ levels, autoionizing in the 6sεd continuum ($l=2$), and the much broader $K=\frac{7}{2}$ and $K=\frac{9}{2}$ levels autoionizing in the 6sεg continuum ($l=4$). The calculated values for the autoionization rates of 5d$_j$5g [K] states are given in table 4.

In figure 3 also the experimental values for the $n=5$–8 autoionization rates are plotted as well as a value for $n=10$ deduced from a dedicated measurement on the $K=\frac{9}{2}$ component. The values obtained for the $K=\frac{9}{2}$ levels (and also for $K=\frac{7}{2}$), are a factor five lower than calculated. The relative autoionization rates within the 5dng configurations are in agreement with calculations. The calculated autoionization rates of the $K=\frac{3}{2}$ and $K=\frac{5}{2}$ level are low ($\leqslant$0.01 cm^{-1}). Experimentally the width of these components is determined by the bandwidth of the laser.

5. Discussion

The experimental autoionization rates are significantly lower than calculated values. In the theoretical model several assumptions are made. First of all exchange effects are neglected. It is easy to show that for 5dng states the exchange induced contribution to autoionization corresponds to a higher order process ($k=4$) and consequently is orders of magnitude smaller than the contribution of the direct electrostatic interaction. The assumption that the inner electron is always closer to the core than the outer electron is justified since the classical inner turning point of the hydrogenic ng electron is 10 a_0 for large n and even larger for low n, while the classical outer turning point of a 5d electron ($n^*=2.4$) moving in the field of a 2^+ core is 3 a_0. Good agreement is found for the relative autoionization rates of the $K=\frac{7}{2}$ and $\frac{9}{2}$ levels autoionizing in the

6sεg continuum. Unfortunately the 5dng $K=\frac{11}{2}$ $J=5$ levels autoionizing in the 6sεi continuum could not be excited from the 5d6p $^3F_4$ state because the wavefunction of the initial state written in a $(jl)K$-coupled basis only contains 5d4f $K=\frac{7}{2}$ components. Since a $\Delta K=2$ transition is forbidden this results in zero transition probability (see table 2). The low autoionization rates of the 5dng $K=\frac{3}{2}$ and $K=\frac{5}{2}$ levels interacting with 6sεd continua result in observed linewidths close to laser linewidth. The fact that $K=\frac{3}{2}$ and $\frac{5}{2}$ levels are much longer lived than $K=\frac{7}{2}$ and $\frac{9}{2}$ levels indicates that the dependence on fine structure is correctly reproduced in the calculations.

The ratio of calculated and experimental linewidths is about 5, independent of n ($n=5$–8, 10). This might hint at a problem in the computation of radial matrix elements in equation (7). An experimental value for the bound quadrupole matrix element may be deduced from the lifetime of the metastable $5d_{5/2}$ ion, $\tau=34.5\pm3.5$ s (Sankey and Madej 1989), giving $\langle 6s|r^2|5d\rangle=14.8\pm0.8\ a_0^2$. This is in agreement with the theoretical value (14.01 a_0^2) used in the calculations. For the computation of Rydberg matrix elements hydrogen wavefunctions are used for the ng electron and regular Coulomb wavefunctions to describe the slow electrons ($\varepsilon=50$–500 meV) rather than plane waves as in the case of fast ejected electrons. The non-zero values of the quantum defects of the 5dng states ($\delta<0.03$) only have a minor influence on the value of the Rydberg matrix element.

The use of single configuration wavefunctions may not be justified as configuration interaction between narrow 5dng states and much broader 5dns and 5dnd states may affect the width of 5dng resonances. In the present work perturbations of the 5dng states do not follow from the quantum defect plots but the occurrence of Fano profiles in the recorded spectra indicates possible mixing with 5dns and 5dnd. However, such an interaction would probably lead to an increase in autoionization rates. Interference effects, that may induce line narrowing in autoionization processes, are known to occur only for specific n-values in a Rydberg series, such as in 5dnd $J=0$ (Neukammer *et al* 1985). In the present case of 5dng this is not the case. Moreover in a multichannel quantum defect study on 5dnd $J=4$ states it was concluded that 5dnd–5dng mixing is negligible (Aymar 1985).

The discrepacy between observed and calculated autoionization rates in the 5dng configuration of barium for $n=5$ makes a comparison with similar configurations in other alkalines-earth of interest. Measurements of 4d5g $J=1$, 2 states in Sr (Jimoyiannis *et al* 1992) and 3d5g $J=1$, 2 states in Ca (Bolovinos *et al* 1992) both show laser linewidth (0.3–0.4 cm^{-1}). These states lie much higher above the first ionization limit and produce faster electrons ($p=0.31$ au, 0.29 au. respectively) than in barium thereby decreasing autoionization rates. When taking calculated values of 12.5 a_0^2 for Sr and 8.6 a_0^2 for Ca for the quadrupole matrix element $\langle d|r^2|s\rangle$ (Poirier 1993) linewidths of 0.57 cm^{-1} and 0.31 cm^{-1} are expected for the $nd_{5/2}5g$ $K=\frac{9}{2}$ $J=4$, 5 states in Sr ($n=4$) and Ca ($n=3$). From the cited experiments no conclusions can be drawn but it would be of interest to investigate these states and those with higher J values with a narrow band laser.

Odd parity $5d_{5/2}n$h $J=5$ series ($n\geqslant20$) of barium were investigated by Bente and Hogervorst (1989b) with a narrow-band CW laser. Examination of linewidths resulted in a scaled autoionization rate $n^3\Gamma$ of 800 GHz. Calculation of scaled autoionization rates within the present theoretical framework results in values of 4000 GHz for the $5d_{5/2}n$h $K=\frac{11}{2}$ component and 2800 GHz for the $K=\frac{9}{2}$ component. Absence of exchange effects due to non-overlapping orbitals also holds for the 5dnh configuration. Fine structure autoionization of $5d_{5/2}n$h levels into $5d_{3/2}\varepsilon l$ continua contributes only 2–3% to the rate of autoionization and can be neglected. Similar to the case of 5dng again a factor of 4–5 discrepancy between theory and experiment exists.

6. Conclusions

From recent work, including the present results, it may be concluded that the model for autoionization in a two electron system, based on the single configuration approximation, applies better in the case of dipolar autoionization than in the case of quadrupolar autoionization. For e.g. 6p*n*f and 6p*n*g states of barium, where many autoionization channels are open, calculations match observed rates satisfactorily. In the much better defined examples of 5d*n*g and 5d*n*h configurations of barium, where only a single continuum plays a role, large discrepancies exist. For the various 5d*j*5g [*K*] states investigated here relative autoionization rates are in good agreement. At present no explanation for the resulting disagreement between theory and experiment has been found. All assumptions made in the theoretical model appear to be justified in 5d*n*g and 5d*n*h configurations. Possibly interactions with other 5d*nl* states are responsible for the low autoionization rates. Future refined experiments on low-lying doubly-excited states in the alkaline-earth atoms, combined with calculations based on realistic interactions between various Rydberg series may clarify this issue.

References

Abutaleb M, De Graaff R J, Ubachs W and Hogervorst W 1991 *Phys. Rev.* A **44** 4187
Aymar M 1985 *J. Phys. B: At. Mol. Phys.* **18** L763
—— 1990 *J. Phys. B: At. Mol. Opt. Phys.* **23** 2697
Bente E A J M and Hogervorst W 1989a *Z. Phys.* D **14** 119
—— 1989b *J. Phys. B: At. Mol. Opt. Phys.* **22** 2679
Bolovinos A, Jimoyiannis A, Assimopoulos S and Tsekeris P 1992 *J. Phys. B: At. Mol. Opt. Phys.* **25** L533
Camus P, Dieulin M, El Himdy A and Aymer M 1983 *Phys. Scr.* **27** 125
Cowan R D 1981 *The Theory of Atomic Structure and Spectra* (Berkeley, CA: University of California Press)
Dai C J, Jaffe S M and Gallagher T F 1989 *J. Opt. Soc. Am.* B **6** 1486
De Graaff R J, Ubachs W and Hogervorst W 1992 *Phys. Rev.* A **45** 166
Greene C H and Aymar M 1991 *Phys. Rev.* A **44** 1773
Greene C H and Kim L 1987 *Phys. Rev.* A **36** 2706
Grundevik P, Lundberg H, Nilsson L and Olsson G 1982 *Z. Phys.* A **306** 95
Jaffe S M, Kachru R, Van Linden van den Heuvel H B and Gallagher T F 1985 *Phys. Rev.* A **32** 1480
Jimoyiannis A, Bolovinos A and Tsekeris P 1992 *Z. Phys.* D **22** 577
Jones R R, Fu P M and Gallagher T F 1991 *Phys. Rev.* A **44** 4260
Lecomte J M, Telmini M, Aymar M and Luc-Koenig E 1994 *J. Phys. B: At. Mol. Opt. Phys.* **27** 667
Luc-Koenig E, Lecomte J M and Aymar M 1994 *J. Phys. B: At. Mol. Opt. Phys.* **27** 699
Neukammer J, Rinneberg H, Jönsson G, Cooke W E, Hieronymus H, König A, Vietzke K and Springer-Bolk H 1985 *Phys. Rev. Lett.* **55** 1979
Nikitin S I and Ostrovsky V N 1980 *J. Phys. B: At. Mol. Phys.* **13** 1961
Poirier M 1988 *Phys. Rev.* A **38** 3484
—— 1993 *Z. Phys.* D **25** 117
Pruvost L, Bolovinos A, Camus P, Lecomte J M and Pillet P 1990 *J. Phys. B: At. Mol. Opt. Phys.* **23** L95
Sankey J D and Madej A A 1989 *Laser Spectroscopy IX* ed M S Feld, J E Thomas and A Mooradian (New York: Academic)
Vergès J 1984 Private communication
Wang X and Cooke W E 1993 *Phys. Rev.* A **47** 1778